Check for updates

Growing Li$_2$O$_2$ surfaces on discharge cause electrolyte degradation and capacity loss in Li–O$_2$ batteries

Chloe Chau,[a] Tammy Nimmo,[a] Daniel Dewar, [a] Gregory J. Rees, [a] Chuan Tan,[b] Kieran D. Jones, [c,d] Lee R. Johnson, [c,d] Xiangwen Gao*[b] and Peter G. Bruce *[a,e]

Ether-based solvents have shown promise as the most stable candidates for the electrolyte solution in the Li–O$_2$ battery. However, the yield of Li$_2$O$_2$ after discharge is less than 100%, despite achieving a near-ideal ratio of charge passed to O$_2$ consumed (2e$^-$/O$_2$) for the reduction of O$_2$ to Li$_2$O$_2$. The loss of Li$_2$O$_2$ leads to the observed capacity fade on cycling and is associated with electrolyte degradation. Here we investigate the chemical formation of Li$_2$O$_2$ from superoxide in two commonly used ether solutions, dimethoxyethane and tetraethylene glycol dimethyl ether. The results indicate that it is the freshly growing Li$_2$O$_2$ surface reacting with the electrolyte solution that is the dominant source of Li$_2$O$_2$ loss and electrolyte degradation. Additionally, we quantify common side products from the degradation, including Li$_2$CO$_3$, HCO$_2$Li, CH$_3$CO$_2$Li and H$_2$O, and identify the composition of ethylene oxides formed during the reaction.

Broader context

The current state of the art in lithium-ion battery technology is approaching its theoretical capacity limit in terms of the energy delivered per unit mass. Li–O$_2$ batteries represent one of the most promising alternatives beyond lithium-ion systems. Li–O$_2$ batteries have attracted considerable research interest due to their exceptionally high theoretical specific energy of 3505 Wh kg^{-1} of Li$_2$O$_2$, which is approximately 6–8 times greater than that of conventional lithium-ion batteries. However, electrolyte degradation remains a significant challenge, as it limits the cycle life and practical viability of Li–O$_2$ cells. The aim of this work is to identify the primary causes of capacity fade during discharge and cycling, and to help consolidate research efforts towards the development of durable and commercially competitive Li–O$_2$ battery technologies.

Introduction

Among the challenges that face the Li–O$_2$ battery, arguably the greatest are degradation and the associated capacity fade on cycling.[1–3] On discharge, the desired reaction at the cathode is the reduction of O$_2$ to Li$_2$O$_2$, with the process being reversed on charge. The most stable electrolyte solutions to date are based on ethers.[4–6] However, even in such electrolytes, the yield of Li$_2$O$_2$ on discharge is less than 100%, resulting in

capacity loss on cycling and the formation of a range of side-reaction products, involving decomposition of the electrolyte solution.[7–9]

Li$_2$CO$_3$, HCO$_2$Li, CH$_3$CO$_2$Li, ethylene oxides and H$_2$O have all been identified as degradation products after cycling.[10–15] The origin of degradation and low Li$_2$O$_2$ yields on discharge has been attributed to possible reactions involving LiO$_2$, the intermediate in the O$_2$/Li$_2$O$_2$ reaction, and singlet oxygen (^{1}O$_2$), the latter of which is produced during disproportionation of LiO$_2$.[16–24] In this work, we show that electrolyte degradation does not arise significantly from reactivity with the LiO$_2$ intermediate. We also confirm the results of a recent study of chemically generated ^{1}O$_2$ with ether electrolytes, which suggested that ^{1}O$_2$ does not react significantly with the electrolyte.[25] Instead, degradation arises from the reactivity between the growing Li$_2$O$_2$ surface and the electrolyte solution, with degradation competing successfully against Li$_2$O$_2$ particle growth. Degradation is greater in tetraethylene glycol dimethyl ether (TEGDME) than in dimethoxyethane (DME). This is due

aDepartment of Materials, University of Oxford, Parks Road, Oxford, OX1 3PH, UK. E-mail: peter.bruce@materials.ox.ac.uk
bFuture Battery Research Centre, Global Institute of Future Technology, Shanghai Jiao Tong University, Shanghai 200240, China
cNottingham Applied Materials and Interfaces Group, School of Chemistry, University of Nottingham, Nottingham, UK
dThe Faraday Institution, Quad One, Harwell Science and Innovation Campus, Didcot OX11 0RA, UK
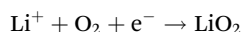*eDepartment of Chemistry, University of Oxford, Oxford, UK*

to the slower formation of Li_2O_2 in TEGDME, in accord with the higher viscosity of the solution and therefore slower diffusivity of species reacting in TEGDME. The role of kinetics is reinforced by observations in Li–O_2 cells that show higher current rates leading to less degradation, as expected from processes that involve the growing Li_2O_2 surface. The quantities of the main degradation products (Li_2CO_3, HCO_2Li, CH_3CO_2Li and H_2O) and the composition of the ethylene oxide species that form from side reactions with ethers are determined.

Results and discussion
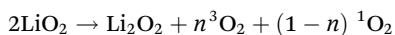
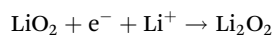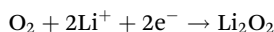The reduction of O_2 to form Li_2O_2 at the cathode is a two-step process:

Step 1:

$$Li^+ + O_2 + e^- \rightarrow LiO_2$$

Step 2(a) – spontaneous disproportionation:

$$2LiO_2 \rightarrow Li_2O_2 + n\,{}^3O_2 + (1-n)\,{}^1O_2$$

Or 2(b) – 2nd electron reduction:

$$LiO_2 + e^- + Li^+ \rightarrow Li_2O_2$$

Overall:

$$O_2 + 2Li^+ + 2e^- \rightarrow Li_2O_2$$

The overall reaction results in a ratio of charge passed to O_2 consumed of 2e$^-$/O_2. It has been shown previously that the dominant reaction on discharge is the consumption of O_2 in the ideal 2e$^-$/O_2 ratio.[26–28] To affirm this, cells were constructed as described in the Methods and discharged with *in situ* gas monitoring. The amount of O_2 consumed is plotted against the charge passed and the dotted line corresponds to the predicted 2e$^-$/O_2 ratio for the O_2/Li_2O_2 reaction, which these cells adhered to within experimental errors (DME: 2.02 ± 0.02; TEGDME: 2.03 ± 0.02) (Fig. S1), in accord with previous studies.[26–28] The significance of adherence to the 2e$^-$/O_2 ratio is that there can be very little reaction between the superoxide intermediate, LiO_2, and the electrolyte solution or carbon electrode. Had such a reaction taken place, the overall amount of O_2 consumed would deviate from the ideal ratio of 2e$^-$/O_2. The results are also consistent with singlet oxygen, which is known to be generated as LiO_2 disproportionates to form Li_2O_2, not playing a significant role in electrolyte or carbon electrode degradation on discharge. If it did so, again the overall amount of O_2 consumed would deviate from the theoretical 2e$^-$/O_2.

Despite the well-acknowledged 2e$^-$/O_2 ratio within the field, many researchers still report and suggest that superoxide and singlet oxygen could play a significant role in Li_2O_2 loss.[17,20,29,30] To confirm the lack of O_2^- or $^1O_2$ reactivity during the formation of Li_2O_2, the latter was generated chemically by adding a solution of LiTFSI in DME or TEGDME to KO_2 powder while stirring. The evolution of O_2 was followed by

online mass spectrometry, as described in the Methods. The reaction is:

$$2KO_2 + 2Li^+ \rightarrow Li_2O_2 + 2K^+ + O_2$$
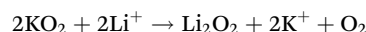
The experiments were conducted with and without 9,10-dimethylanthracene (DMA), a trap for $^1O_2$, and the results are shown in Fig. 1. 100% O_2 evolution would correspond to the quantity expected if all the KO_2 reacted to form Li_2O_2 (*i.e.* the lithium electrolyte solution was in excess in all cases). The amount of O_2 detected in the absence of the trap is very close to 100% for both DME (99.7 ± 0.2%) and TEGDME (99.8 ± 0.2%) as shown in Fig. 1(a). If O_2^- or $^1O_2$ had reacted with the electrolyte solution, then the O_2 yield would be below 100%. These results further confirm that neither O_2^- nor $^1O_2$ are major sources of degradation. These are more challenging conditions under which O_2^- might have reacted with the electrolyte solution than in Li–O_2 cells since KO_2 persists in the solution longer than the transient formation of LiO_2 during O_2 reduction to Li_2O_2 in cells due to the greater solubility of the former over the latter.[31,32] In the presence of the trap, $^1O_2$ is quenched to form DMA–O_2 and the mass spectrometer detects only $^3O_2$, leading to less O_2 detected in both cases (98.6 ± 0.2% in DME and 95.4 ± 0.2% in TEGDME). By comparing the yield of O_2 with and without the trap, we confirm that $^1O_2$ is indeed formed in the reaction and that the amount of $^1O_2$ produced is
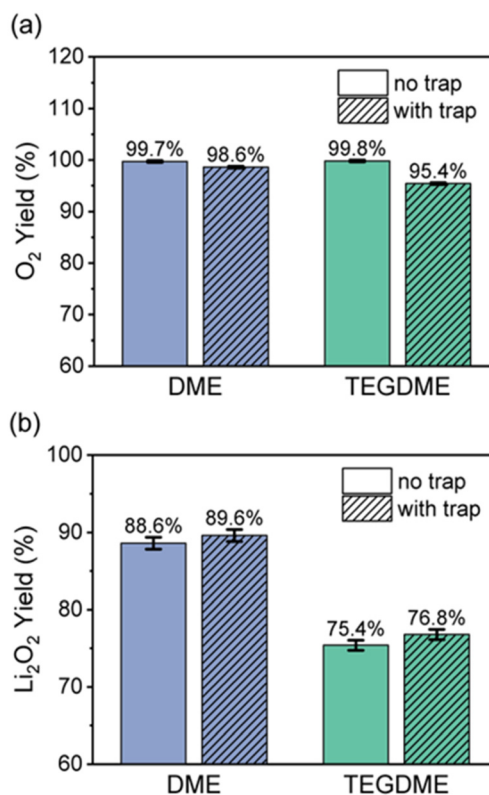

Fig. 1 (a) Oxygen and (b) Li_2O_2 yields after KO_2 disproportionation in DME (blue) and TEGDME (green) without and with singlet oxygen trap, showing no evidence of $^1O_2$ or O_2^- reactivity.

greater in the case of TEGDME (4.4 ± 0.3%) compared with DME (1.1 ± 0.3%). Yet even this greater amount of $^1O_2$ does not induce observable degradation in the case of TEGDME. The yield of Li_2O_2 was determined for the cases of DME and TEGDME with and without a $^1O_2$ trap by photometric titration using $TiOSO_4$.[33,34] The results are shown in Fig. 1(b). In all cases, the Li_2O_2 yield is lower than 100%, as expected given side reactions, but does not vary significantly with and without the $^1O_2$ trap (DME: 89.6 ± 0.8% *vs.* 88.6 ± 0.8%; TEGDME: 76.8 ± 0.7% *vs.* 75.4 ± 0.7%). This further supports the conclusion that singlet oxygen is not a major source of degradation.

The absence of degradation arising from a reaction with O_2^- or $^1O_2$ points to Li_2O_2 as the possible source of degradation. To investigate the reactivity of ethers with already formed Li_2O_2 surfaces, a known amount of Li_2O_2 (synthesised in-house, see Methods) was added separately to solutions of 0.1 M LiTFSI in DME and TEGDME. After 24 hours of stirring, the quantity of Li_2O_2 remaining was determined again by photometric titration. The amounts of Li_2O_2 that remained, as a percentage of the amounts added initially, were 98.0 ± 0.8% (DME) and 97.7 ± 0.8% (TEGDME). This shows that the as-prepared Li_2O_2 does not react with the electrolyte solution to an extent that explains the yield loss both in the chemical disproportionation reaction and on discharge.

The lack of reactivity with already formed Li_2O_2 implies that it is the reaction between the electrolyte solution and the growing surface of the Li_2O_2 particles that is primarily responsible for the Li_2O_2 loss. If it is the freshly growing Li_2O_2 surface that reacts with the electrolyte solution, then the rate of Li_2O_2 particle growth should affect the extent of the side reactions and therefore the yield of Li_2O_2. If particles grow more rapidly, then less time is available for reaction with the electrolyte solution and the degree of degradation should be lower. To investigate this, the rate of Li_2O_2 formation in the two different electrolyte solutions, LiTFSI in TEGDME and DME, were investigated. The same quantity of the electrolyte solution and KO_2 were reacted for both systems with the pressure change monitored as a function of time to follow the O_2 evolution and rate of Li_2O_2 formation. The results are shown in Fig. 2, where it is clear that Li_2O_2 grows significantly more rapidly in DME than in TEGDME, in accord with the higher yield of Li_2O_2 and consequently lower amount of degradation products in the case of DME compared with TEGDME. The formation of larger particles in TEGDME (Fig. S2) is in accord with the slower growth rate. The two solvents have similar donor numbers (20 for DME and 16.6 for TEGDME)[35] and hence similar Li^+ solvation, however the viscosity of TEGDME is much higher than DME (3.73 and 0.42 mPa s respectively)[36] which is primarily responsible for the slower formation of Li_2O_2 and the larger particle sizes observed. Note that despite the larger particles and therefore lower surface area for Li_2O_2 formed in TEGDME, the degradation is greater in TEGDME compared with DME, further emphasising the role of the Li_2O_2 growth kinetics.

The importance of Li_2O_2 growth rate on the Li_2O_2 yield within a single solvent system was also examined. The same KO_2 dispro-
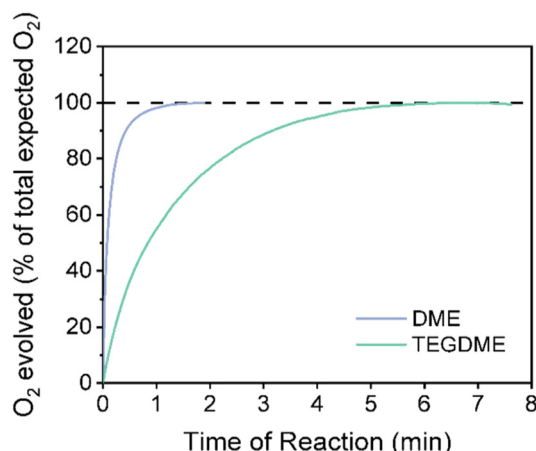

Fig. 2 *In situ* pressure monitoring of the gas evolution during KO_2 disproportionation in DME (blue) and TEGDME (green). The pressure was monitored in a sealed reaction vessel equipped with a pressure transducer, containing KO_2 powder to which an electrolyte of 0.8 M LiTFSI in the relevant solvent was added whilst stirring. The pressure increase was expressed as a percentage of the total pressure increase that would be expected if all the KO_2 reacted to form O_2.

portionation experiments with *in situ* pressure monitoring were performed in TEGDME with the lithium salt concentration modulated from 0.1 M to 2 M to change the reaction rate (Fig. S3). The rate of O_2 evolution increased with increasing salt concentration, Fig. S3(a), while simultaneously the Li_2O_2 yield also increased, Fig. S3(b). This reinforces the conclusion that the Li_2O_2 growth rate is a critical factor that governs the overall extent of degradation and final Li_2O_2 yield in ethers. Consistent with the growth rate, the morphology of the products showed smaller particles formed with higher salt concentration as the nucleation of Li_2O_2 was more rapid (Fig. S4).
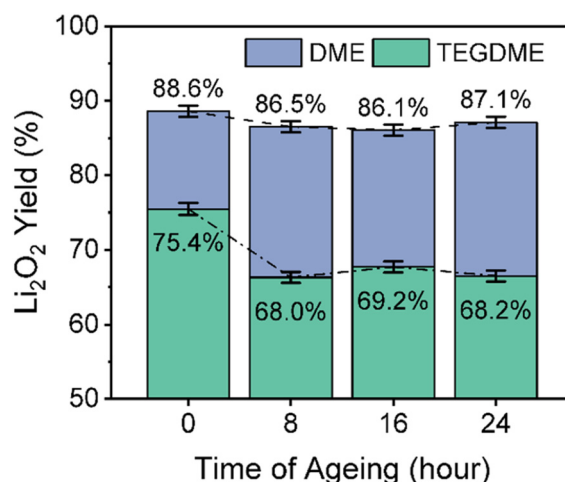

Fig. 3 Quantity of Li_2O_2 as a percentage of the theoretical yield of Li_2O_2 after the KO_2 disproportionation reaction, in DME (blue) and TEGDME (green), has gone to completion. The quantity of Li_2O_2 was determined immediately after the reaction was complete (0 hours), and after a further 8, 16 and 24 hours of ageing.

As well as the rate of Li_2O_2 particle growth, the degree of Li_2O_2 loss will depend on the rate of reaction between the growing Li_2O_2 surface and the electrolyte solution. To probe this, after the reaction between the lithium electrolyte solutions (0.8 M LiTFSI) and KO_2 went to completion in DME and TEGDME (*i.e.* the time at which O_2 evolution had reached the plateau in Fig. 2), the quantity of Li_2O_2 was monitored as a function of time (Fig. 3). There is very little change in the amount of Li_2O_2 in the case of DME, but for TEGDME, the amount of Li_2O_2 continues to decrease in the first 8 hours, indicating further degradation on a slower timescale than in DME. Despite the slower reaction between Li_2O_2 and TEGDME compared with DME, the Li_2O_2 yield in TEGDME is lower, indicating that the increased length of exposure time of the freshly growing Li_2O_2 surface due to the slow Li_2O_2 growth in TEGDME is largely responsible for the difference in yield.

While the products of degradation associated with O_2 reduction on discharging Li–O_2 cells with ether-based electrolytes have been identified previously, here we quantify their relative amounts and compare them for the disproportionation of KO_2 with LiTFSI in DME and TEGDME respectively.[13–15] Full experimental details of the characterisation procedures are provided in the Methods. PXRD and FTIR spectra of the collected solid products at the end of the reaction are shown in Fig. 4a and b. They confirm the formation of Li_2O_2 as the main product along with Li_2CO_3, HCO_2Li and CH_3CO_2Li as the side products in both DME and TEGDME. Solid-state ^{13}C NMR identified the presence of ethylene oxides as an additional side-product (Fig. 4c). Following an established procedure, the peaks corresponding to the terminal $–CH_3$ and chain $–CH_2$ moieties were integrated, and by taking the ratios of the integrated areas, the ethylene oxide species detected were confirmed to have different average chain lengths in the two electrolytes; $CH_3(OCH_2CH_2)_{1.3}OCH_3$ for DME and $CH_3(OCH_2CH_2)_{4.8}OCH_3$ for TEGDME.[37] Solution ^{1}H NMR spectra of the electrolytes after disproportionation of the KO_2 powder show no evidence of solution-soluble organic products (Fig. S5). Karl Fischer titrations of electrolytes after the reac-
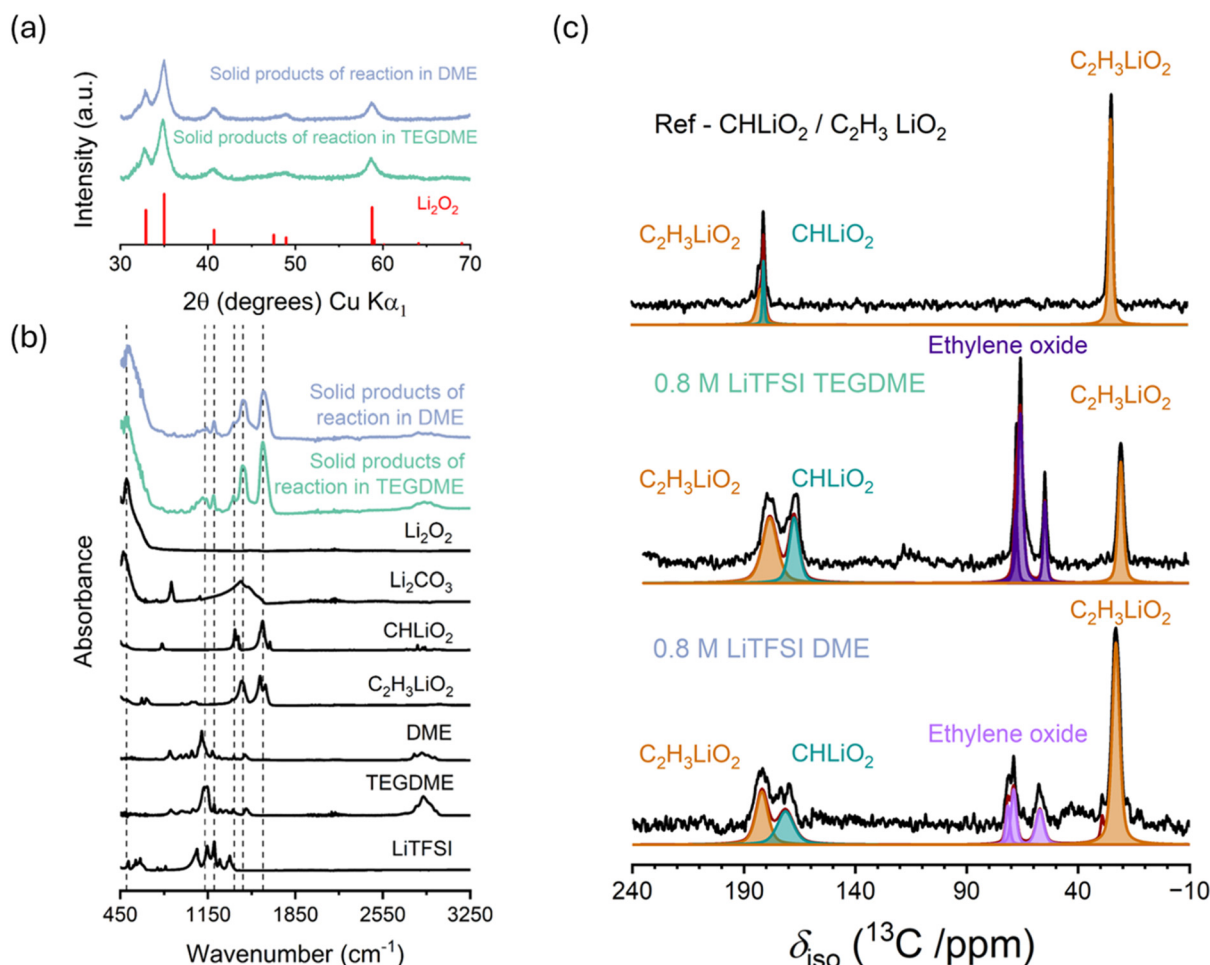

Fig. 4 (a) PXRD, (b) ATR-FTIR and (c) solid-state ^{13}C NMR spectra of solid products formed from KO_2 disproportionation in an electrolyte of 0.8 M LiTFSI in DME (blue) and TEGDME (green). PXRD shows Li_2O_2 is the main solid product with side products identified through ATR-FTIR as lithium formate, acetate, carbonate, and residual ether solvent molecules. Solid-state ^{13}C NMR spectra of the solid products are compared to reference spectra of 1 : 1 commercial $C_2H_3LiO_2$ and $CHLiO_2$, showing side products formed from degradation of Li_2O_2 and glyme solvent, identified as lithium formate, acetate and ethylene oxides.

tions show the formation of H_2O as a product of degradation (Fig. 5).

The amount of Li_2CO_3 formed was determined using mass spectroscopy to quantify the amount of CO_2 evolved from its stoichiometric reaction with H_3PO_4. HCO_2Li and CH_3CO_2Li were quantified by ^1H NMR of the dissolved solid product in D_2O, as described in the Methods. The amount of Li_2CO_3, HCO_2Li and CH_3CO_2Li and H_2O are reported in Fig. 5. They are expressed as mole percentages of the theoretical amount of Li_2O_2 expected from the quantity of KO_2 used in the reaction. The amount of side products identified is greater in the case of TEGDME than in DME, in accord with the lower Li_2O_2 yield in TEGDME. HCO_2Li is the dominant degradation product in both DME and TEGDME. The order of the prevalence of the side products, HCO_2Li, CH_3CO_2Li, H_2O and Li_2CO_3, are also similar.

We propose the origin of these degradation products to be by a surface confined hydrogen atom transfer (HAT) reaction at a secondary carbon site by Li_2O_2, forming an α-alkoxyalkyl radical and hydroperoxide (Fig. 6). This initiation step is well

supported computationally, where facile dissociation of hydroperoxide to an electron rich Li–O–Li site and hydroxide (a potential source of H_2O) is suggested.[38,39] The resulting α-alkoxyalkyl radical participates in complex branching pathways, with two initial stages.[40,41] Firstly, radical recombination with an oxo-species gives hemiacetal-type structures, which are susceptible to base-mediated decomposition yielding reactive aldehydic compounds.[38,39] Simultaneously, β-scission of the alkyloxy radical intermediate is known to yield carbonyl compounds while releasing a carbon-centred radical.[40,42] The latter propagates further reactions such as HAT or terminating radical processes which may account for contracted or extended ethylene oxides.[43] Both summarised pathways produce carbonyl bearing compounds which are susceptible to multiple degradation routes including enolisation to formate and alkoxides,[44] and reactions with peroxides, such as the Baeyer–Villiger or Dakin oxidations, that tend to yield carboxylates, *gem*-dihydroperoxides, or similar hemiacetal functionality.[11,45,46] Ultimately, the journey following HAT of the parent ether is nonlinear, eventually arriving at the common terminus of fragmented and highly oxidised hydrocarbons (formate, acetate, carbonate, *etc.*), coupled with the release of water. Although the yield of Li_2O_2 and the amount of these degradation products can be determined, the number of possible branching degradation pathways, and volatile organic intermediates formed, makes it difficult to rationalise the relationship between the two. Furthermore, the reactivity between the solvent and the Li_2O_2 surface could depend on which Li_2O_2 surface facets are exposed, which in turn depends on the growth rate of the peroxide.[38,39,47–49] Disentangling these different phenomena is beyond the scope of this work, but future avenues for investigation are discussed more fully in SI Note 1.

Given that the differences in the rates of Li_2O_2 formation between DME and TEGDME play a role in the extent of degradation, this implies that degradation will depend on the rate of discharge in Li–O_2 cells. Electrochemical cells were constructed using 0.8 M LiTFSI in DME and TEGDME as electrolytes, as described in the Methods. The DME cells were discharged at two different rates and the TEGDME cell was dis-
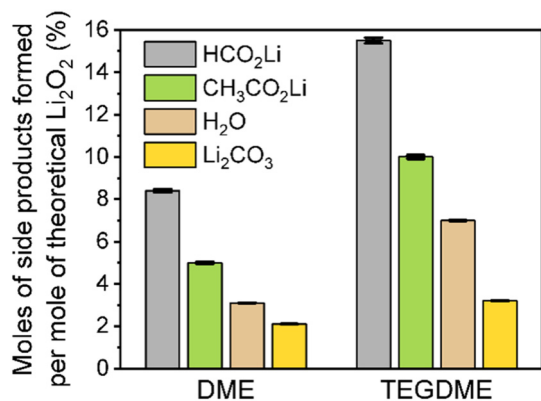

Fig. 5 Moles of side-reaction products (HCO_2Li, CH_3CO_2Li, H_2O and Li_2CO_3) quantified in the product formed from KO_2 disproportionation in the electrolytes of 0.8 M LiTFSI in DME and TEGDME. The quantities of each side-reaction product are expressed as a percentage of the theoretical number of moles of Li_2O_2 expected from the disproportionation reaction when all the KO_2 reacts.
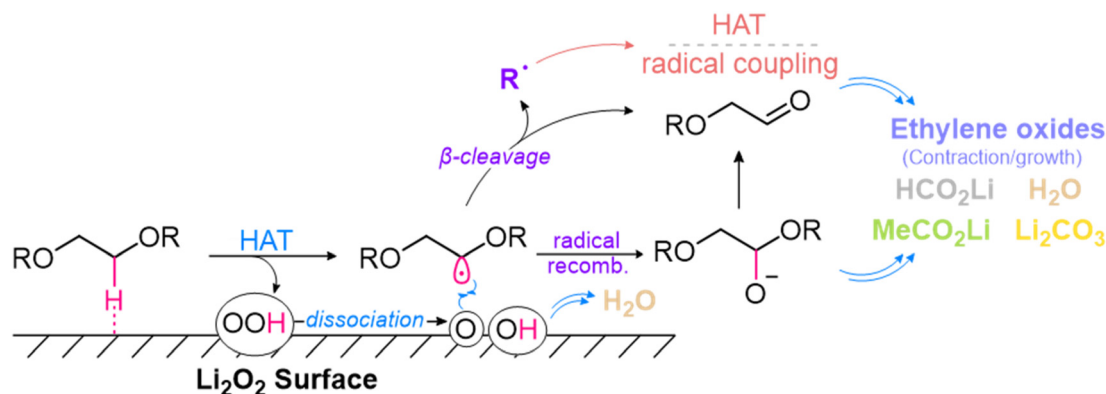

Fig. 6 Summary of the proposed degradation pathway of alkyl ethers at the Li_2O_2 surface.

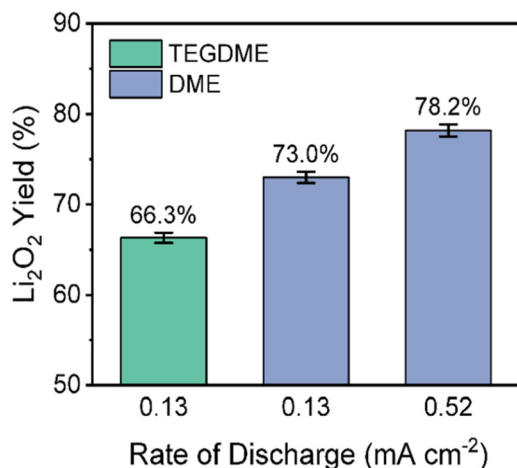**Fig. 7** Li_2O_2 yield quantified in cathodes discharged in electrolytes of 0.8 M LiTFSI in DME (blue) and TEGDME (green). Cells were discharged under O_2 at 0.13 mA cm^{-2} and 0.52 mA cm^{-2} in DME and 0.13 mA cm^{-2} in TEGDME to a fixed capacity of 5.2 mA h cm^{-2}. The Li_2O_2 yield is expressed as a percentage of the theoretical moles of Li_2O_2 expected for the amount of charge passed following an ideal 2e$^-$/Li_2O_2 reaction.

charged at the lower of the two rates. All were discharged to the same fixed capacity. The TEGDME cell could not reach this capacity at the higher rate. The yields of Li_2O_2 at the end of discharge were determined and are reported in Fig. 7. The higher rate of discharge, 0.52 mA cm^{-2} compared with 0.13 mA cm^{-2} in DME, resulted in a higher Li_2O_2 yield. TEGDME, compared with DME at the same lower discharge rate resulted in a lower Li_2O_2 yield.

The discharged cathodes were characterised using the same methods as for the solid products of KO_2 disproportionation, which revealed identical side-products formed in both cases (Fig. S6 and S7). Unlike the KO_2 chemical results, when formed electrochemically the growth rate of Li_2O_2 is controlled by the current density which in turn controls the morphology of the products. Similar toroidal particles were produced on cathodes discharged at the same current density of 0.13 mA cm^{-2} in both DME and TEGDME (Fig. S8), emphasising that it is the rate of growth that primarily determines the particle size. From previous studies, it is known that increasing the discharge current rate tends to smaller Li_2O_2 particle sizes and smaller capacities.[48,50] While faster discharge and hence growth of Li_2O_2 may therefore provide a strategy to mitigate degradation to an extent, this is not a practical solution to the problem as large capacities at different discharge currents are required in a cell in practice. The results of this study therefore highlight that improving solvent stability is the critical requirement to achieving a competitive cycle life in Li–O_2 cells.

Conclusions

Loss of Li_2O_2 (*i.e.* low yields) and degradation of the electrolyte arise from the reaction between the growing surfaces of Li_2O_2

particles and the electrolyte. There is no evidence that O_2^- or singlet O_2 play a significant role in the electrolyte degradation or low Li_2O_2 yield. The Li_2O_2 growth rate in dimethoxyethane is faster and the degree of electrolyte degradation is lower than that in tetraethylene glycol dimethyl ether, in accord with the lower viscosity of dimethoxyethane. This work expands upon previous studies by showing that the relative prominence of the degradation products, Li_2CO_3, HCO_2Li, CH_3CO_2Li and H_2O are similar in both solvents, emphasising that the rate of Li_2O_2 formation only affects the overall extent of degradation. The composition of the ethylene oxide species that form was also determined for both solvents. By demonstrating that the origin of degradation and loss of Li_2O_2 (*i.e.* low yields) arises from the reaction between the growing Li_2O_2 particle surfaces and the electrolyte solution, and not from O_2^- or singlet O_2, we direct future research towards informed electrolyte solvent design with an emphasis on stability at the growing Li_2O_2 surface, potentially leading to an improvement in Li–O_2 cell cycle life.

Experimental

Materials and methods

Bis(trifluoromethane)sulfonyl imide lithium salt (LiTFSI), 1,2-dimethoxyethane (DME), tetraethylene glycol dimethyl ether (TEGDME), 9,10-dimethylanthracene (DMA) were purchased from Sigma Aldrich. DME and TEGDME were dried over activated molecular sieves (type 4 Å, Aldrich) before use. LiTFSI was dried at 120 °C under vacuum for 3 days before transferring and storage inside an Ar-filled glovebox (H_2O and O_2 content ~1 ppm). The water content of all electrolyte solutions formed within the salt and solvent was <8 ppm, determined by Karl-Fischer (KF) titration. Potassium dioxide (KO_2) and lithium formate monohydrate were purchased from Sigma Aldrich, and lithium acetate and lithium carbonate were purchased from Thermo Scientific. Li_2O_2 was synthesised in-house following established methods as reported previously.[51,52] All materials were stored in an Ar-filled glovebox before use.

Chemical disproportionation reaction

Chemical disproportionation of KO_2 to Li_2O_2 in Li$^+$-containing electrolytes was carried out by reacting samples of 3.0 mg of KO_2 powder with 1 mL of 0.8 M LiTFSI in DME or TEGDME under stirring. *In situ* pressure monitoring during disproportionation was used to determine the reaction kinetics and the time taken to reach the endpoint of the reaction in each electrolyte. The pressure was monitored in a sealed reaction vessel equipped with a pressure transducer (Omega Engineering Ltd). The time for the reaction to reach completion was marked by the time at which the pressure stopped increasing, indicating no further O_2 evolution.

The amount of O_2 liberated during the reaction was quantified by online mass spectrometry (Thermo Scientific) using Ar carrier gas at a flow rate of 1 mL min^{-1}. The Li_2O_2 yield was

quantified by photometric titration with UV-vis spectrometry (Thermo Fisher Evolution 220), following a method reported previously.[33,34] The UV-vis absorbance was calibrated against solutions containing known amounts of Li_2O_2, to which the same quantity of electrolyte was added as was present in the reaction mixtures to correct for its contribution to the absorbance signal. Errors in determining the Li_2O_2 and O_2 yields are estimated based on the errors from the gas flow regulator, weighing of KO_2 powder and pipetting.

Electrochemical measurements

Airtight Swagelok-type Li–O_2 cells were assembled as reported previously[12] and consisted of a porous carbon gas diffusion cathode to which high-purity O_2 (BOC, N5.5) was supplied in a sealed tube. 3 glass fiber separators (Whatman GF/C) of 13 mm diameter were filled with 250 μL of electrolyte and a partially oxidised $LiFePO_4$ electrode was used as a substitute for a Li–metal anode. When partially delithiated, Li_xFePO_4 has a fixed potential of 3.45 V vs. Li^+/Li and is stable in contact with the electrolyte solution. The remaining de-lithiation capacity of the Li_xFePO_4 electrode was ensured to be greater than the targeted discharge capacity of the cathodes. The use of such a Li_xFePO_4 electrode has been described previously.[12] The porous cathodes were composed of carbon black (Super P, Alfa Aesar), which was pre-treated under an Ar : H_2 (95 : 5 v/v) gas at 900 °C for 6 hours, and PTFE binder (Sigma-Aldrich) in an 85 : 15 w/w ratio. The electrodes were prepared from a slurry of carbon and PTFE (60 wt% dispersion in H_2O) in isopropanol, which was dried, and the resulting mixture was pressed into 5 mm diameter discs of 2.0 mg mass. All electrodes and cell components were dried at 120 °C under vacuum for 24 hours before use and were stored in an Ar-filled glovebox without exposure to air. Cells were assembled and discharged inside the glovebox. Galvanostatic discharge was carried out using a VMP3 Biologic potentiostat. In situ pressure monitoring during discharge was performed by attaching a pressure transducer to the airtight Swagelok-type cell. After discharge, a similar protocol was applied to quantify the Li_2O_2 yield in the discharged cathodes using UV-Vis spectroscopy. Discharged cathodes were rinsed with DME twice and dried under vacuum at room temperature for further characterisation.

Characterisation and quantification of reaction products

The mixture after the chemical disproportionation reaction was centrifuged and the supernatant filtered through a 1 μm pore glass filter for solution-state ^{1}H nuclear magnetic resonance (NMR) analysis on a 600 MHz Bruker spectrometer. The solids after centrifugation were rinsed with DME twice before drying under vacuum at room temperature. Powder X-ray diffraction (PXRD) patterns of dried solids were acquired using a Rigaku Miniflex X-ray diffractometer and ATR-FTIR spectra were acquired with a Thermo Fisher Nicolet iS50 spectrometer, both in a N_2-filled glovebox. Solid-state ^{13}C NMR spectra were acquired with a 400 MHz Bruker spectrometer, where dried solids were packed into an airtight sample holder before being transported outside of the glovebox for measurements. The

morphologies of the solid products were observed by FE-SEM (Zeiss-Merlin) with an airtight transfer to avoid any exposure to air.

The amount of Li_2CO_3 in the dried solids and dried cathodes were quantified by treating them with 1 M H_3PO_4 (which reacts specifically with Li_2CO_3, not the organic carbonates) and monitoring the CO_2 evolution by online mass spectrometry using Ar carrier gas at a flow rate of 1 mL min^{-1}. HCO_2Li and CH_3CO_2Li in the solids were quantified by solution-state ^{1}H NMR measurements. 5 mg of the solid was dissolved in 1 mL D_2O, and the solutions sealed inside airtight J-Young NMR tubes in an Ar-filled glovebox for measurement on a 600 MHz Bruker spectrometer equipped with a cryoprobe. Calibration curves were obtained from reference samples of HCO_2Li and CH_3CO_2Li of known concentrations. The amount of Li_2CO_3, HCO_2Li and CH_3CO_2Li per unit mass of solid product formed is then correlated to the Li_2O_2 yield through quantifying the amount of Li_2O_2 in a unit mass of solid product. An equivalent protocol was applied to discharged cathodes for analysis of the side product species formed after discharge.

Author contributions

C. C. performed chemical and electrochemical measurements. C. C. and T. N. performed pressure monitoring measurements on chemical disproportionation reaction and analysed the data. C. C. characterised reaction products and discharged cathodes with contributions from T. N. and D. D. D. D. performed pressure monitoring measurements on discharge and analysed the data. G. R. performed solid state NMR measurements and analysed the data. C. C., D. D., C. T., and T. N. analysed data. K. J. and L. J. analysed data and visualised the degradation mechanism. P. G. B., X. G., C. C., and D. D. interpreted the data. X. G. and P. G. B. wrote the manuscript with contributions from D. D., C. T., and C. C.

Conflicts of interest

There are no conflicts to declare.

Data availability

The datasets used and analysed during the current study are available from the corresponding author upon reasonable request.

Supplementary information is available. See DOI: https://doi.org/10.1039/d5eb00137d.

Acknowledgements

References

1 J. Lai, Y. Xing, N. Chen, L. Li, F. Wu and R. Chen, *Angew. Chem., Int. Ed.*, 2020, **59**, 2974–2997.

2 J. Ma, Y. Li, N. S. Grundish, J. B. Goodenough, Y. Chen, L. Guo, Z. Peng, X. Qi, F. Yang, L. Qie, C.-A. Wang, B. Huang, Z. Huang, L. Chen, D. Su, G. Wang, X. Peng, Z. Chen, J. Yang, S. He, X. Zhang, H. Yu, C. Fu, M. Jiang, W. Deng, C.-F. Sun, Q. Pan, Y. Tang, X. Li, X. Ji, F. Wan, Z. Niu, F. Lian, C. Wang, G. G. Wallace, M. Fan, Q. Meng, S. Xin, Y.-G. Guo and L.-J. Wan, *J. Phys. D: Appl. Phys.*, 2021, **54**, 183001.

3 B. D. Adams, R. Black, Z. Williams, R. Fernandes, M. Cuisinier, E. J. Berg, P. Novak, G. K. Murphy and L. F. Nazar, *Adv. Energy Mater.*, 2015, **5**, 1400867.

4 H.-G. Jung, J. Hassoun, J.-B. Park, Y.-K. Sun and B. Scrosati, *Nat. Chem.*, 2012, **4**, 579–585.

5 W. Yu, H. Wang, J. Hu, W. Yang, L. Qin, R. Liu, B. Li, D. Zhai and F. Kang, *ACS Appl. Mater. Interfaces*, 2018, **10**, 7989–7995.

6 V. S. Bryantsev, V. Giordani, W. Walker, M. Blanco, S. Zecevic, K. Sasaki, J. Uddin, D. Addison and G. V. Chase, *J. Phys. Chem. A*, 2011, **115**, 12399–12409.

7 K. U. Schwenke, M. Metzger, T. Restle, M. Piana and H. A. Gasteiger, *J. Electrochem. Soc.*, 2015, **162**, A573–A584.

8 L.-N. Song, L.-C. Zou, X.-X. Wang, N. Luo, J.-J. Xu and J.-H. Yu, *iScience*, 2019, **14**, 36–46.

9 B. D. McCloskey, J. M. Garcia and A. C. Luntz, *J. Phys. Chem. Lett.*, 2014, **5**, 1230–1235.

10 S. A. Freunberger, Y. Chen, N. E. Drewett, L. J. Hardwick, F. Bardé and P. G. Bruce, *Angew. Chem., Int. Ed.*, 2011, **50**, 8609–8613.

11 J. M. Garcia, H. W. Horn and J. E. Rice, *J. Phys. Chem. Lett.*, 2015, **6**, 1795–1799.

12 X. Gao, Y. Chen, L. R. Johnson, Z. P. Jovanov and P. G. Bruce, *Nat. Energy*, 2017, **2**, 17118.

13 R. Younesi, M. Hahlin, F. Björefors, P. Johansson and K. Edström, *Chem. Mater.*, 2013, **25**, 77–84.

14 D. Sharon, V. Etacheri, A. Garsuch, M. Afri, A. A. Frimer and D. Aurbach, *J. Phys. Chem. Lett.*, 2013, **4**, 127–131.

15 B. D. Mccloskey, A. Valery, A. C. Luntz, S. R. Gowda, G. M. Wallraff, J. M. Garcia, T. Mori and L. E. Krupp, *J. Phys. Chem. Lett.*, 2013, **4**, 2989–2993.

16 R. Black, S. H. Oh, J.-H. Lee, T. Yim, B. Adams and L. F. Nazar, *J. Am. Chem. Soc.*, 2012, **134**, 2902–2905.

17 W.-J. Kwak, J.-B. Park, H.-G. Jung and Y.-K. Sun, *ACS Energy Lett.*, 2017, **2**, 2756–2760.

18 X. Gao, Y. Chen, L. Johnson and P. G. Bruce, *Nat. Mater.*, 2016, **15**, 882–888.

19 A. C. Luntz and B. D. Mccloskey, *Nat. Energy*, 2017, **2**, 17056.

20 N. Mahne, B. Schafzahl, C. Leypold, M. Leypold, S. Grumm, A. Leitgeb, G. A. Strohmeier, M. Wilkening, O. Fontaine, D. Kramer, C. Slugovc, S. M. Borisov and S. A. Freunberger, *Nat. Energy*, 2017, **2**, 17036.

21 W.-J. Kwak, Rosy, D. Sharon, C. Xia, H. Kim, L. R. Johnson, P. G. Bruce, L. F. Nazar, Y.-K. Sun, A. A. Frimer, M. Noked, S. A. Freunberger and D. Aurbach, *Chem. Rev.*, 2020, **120**, 6626–6683.

22 X. Wu, B. Niu, H. Zhang, Z. Li, H. Luo, Y. Tang, X. Yu, L. Huang, X. He, X. Wang, Y. Qiao and S. G. Sun, *Adv. Energy Mater.*, 2023, **13**, 2203089.

23 A. Petrongari, V. Piacentini, A. Pierini, P. Fattibene, C. De Angelis, E. Bodo and S. Brutti, *ACS Appl. Mater. Interfaces*, 2023, **15**, 59348–59357.

24 Z. Jiang, Y. Huang, Z. Zhu, S. Gao, Q. Lv and F. Li, *Proc. Natl. Acad. Sci. U. S. A.*, 2022, **119**, 1–6.

25 C. Zor, K. D. Jones, G. J. Rees, S. Yang, A. T. R. Pateman, X. Gao, L. Johnson and P. G. Bruce, *Energy Environ. Sci.*, 2024, **17**, 7355–7361.

26 S. Dong, S. Yang, Y. Chen, C. Kuss, G. Cui, L. R. Johnson, X. Gao and P. G. Bruce, *Joule*, 2022, **6**, 185–192.

27 B. D. McCloskey, D. S. Bethune, R. M. Shelby, G. Girishkumar and A. C. Luntz, *J. Phys. Chem. Lett.*, 2011, **2**, 1161–1166.

28 B. D. McCloskey, D. S. Bethune, R. M. Shelby, T. Mori, R. Scheffler, A. Speidel, M. Sherwood and A. C. Luntz, *J. Phys. Chem. Lett.*, 2012, **3**, 3043–3047.

29 E. Mourad, Y. K. Petit, R. Spezia, A. Samojlov, F. F. Summa, C. Prehal, C. Leypold, N. Mahne, C. Slugovc, O. Fontaine, S. Brutti and S. A. Freunberger, *Energy Environ. Sci.*, 2019, **12**, 2559–2568.

30 Y. K. Petit, E. Mourad, C. Prehal, C. Leypold, A. Windischbacher, D. Mijailovic, C. Slugovc, S. M. Borisov, E. Zojer, S. Brutti, O. Fontaine and S. A. Freunberger, *Nat. Chem.*, 2021, **13**, 465–471.

31 W. Hesse, M. Jansen and W. Schnick, *Prog. Solid State Chem.*, 1989, **19**, 47–110.

32 X. Ren and Y. Wu, *J. Am. Chem. Soc.*, 2013, **135**, 2923–2926.

33 P. Hartmann, C. L. Bender, J. Sann, A. K. Durr, M. Jansen, J. Janek and P. Adelhelm, *Phys. Chem. Chem. Phys.*, 2013, **15**, 11661–11672.

34 B. Schafzahl, E. Mourad, L. Schafzahl, Y. K. Petit, A. R. Raju, M. O. Thotiyl, M. Wilkening, C. Slugovc and S. A. Freunberger, *ACS Energy Lett.*, 2018, **3**, 170–176.

35 Z. Ma, X. Yuan, L. Li, Z.-F. Ma, D. P. Wilkinson, L. Zhang and J. Zhang, *Energy Environ. Sci.*, 2015, **8**, 2144–2198.

36 S. Tang and H. Zhao, *RSC Adv.*, 2014, **4**, 11251–11287.

37 A. Tapash, P. J. DesLauriers and J. L. White, *Macromolecules*, 2015, **48**, 3040–3048.

38 R. S. Assary, K. C. Lau, K. Amine, Y.-K. Sun and L. A. Curtiss, *J. Phys. Chem. C*, 2013, **117**, 8041–8049.

39 N. Kumar, M. D. Radin, B. C. Wood, T. Ogitsu and D. J. Siegel, *J. Phys. Chem. C*, 2015, **119**, 9050–9060.

40 V. S. Kosobutskii, *High Energy Chem.*, 2006, **40**, 277–295.

41 I. Fleming, *Radical Reactions in Molecular Orbitals and Organic Chemical Reactions*, John Wiley & Sons Ltd., 2010, vol. 1, ch. 7, pp. 369–400.

42 K. L. Samony and D. K. Kim, *ChemCatChem*, 2023, **15**, 1–11.

43 L. Capaldo, D. Ravelli and M. Fagnoni, *Chem. Rev.*, 2022, **122**, 1875–1924.

44 J. Kenner and G. N. Richards, *J. Chem. Soc.*, 1953, 2240–2244.

45 C. Hassall, *The Baeyer–Villiger Oxidation of Aldehydes and Ketones*, 2011, vol. 9.

46 N. Tada, L. Cui, H. Okubo, T. Miura and A. Itoh, *Chem. Commun.*, 2010, **46**, 1772.

47 R. R. Mitchell, B. M. Gallant, Y. Shao-Horn and C. V. Thompson, *J. Chem. Phys.*, 2013, **4**, 1060.

48 B. D. Adams, C. Radtke, R. Black, M. L. Trudeau, K. Zaghib and L. F. Nazar, *Energy Environ. Sci.*, 2013, **6**, 1772.

49 T. Laino and A. Curioni, *New J. Phys.*, 2013, **15**, 095009.

50 B. M. Gallant, D. G. Kwabi, R. R. Mitchell, J. Zhou, C. V. Thompson and Y. Shao-Horn, *Energy Environ. Sci.*, 2013, **6**, 2518.

51 T. A. Dobrynina, N. A. Akhapkina and V. F. Chuvaev, *Bull. Acad. Sci. USSR, Div. Chem. Sci.*, 1969, **18**, 438–440.

52 S. Ahn, C. Zor, S. Yang, M. Lagnoni, D. Dewar, T. Nimmo, C. Chau, M. Jenkins, A. J. Kibler, A. Pateman, G. J. Rees, X. Gao, P. Adamson, N. Grobert, A. Bertei, L. R. Johnson and P. G. Bruce, *Nat. Chem.*, 2023, **15**, 1022–1029.